bioRxiv preprint doi: https://doi.org/10.1101/2020.12.06.412304; this version posted December 6, 2020. The copyright holder for this preprint (which was not certified by peer review) is the author/funder. All rights reserved. No reuse allowed without permission.

Genetically Engineered Integral Feedback Controllers for Robust Perfect Adaptation in Mammalian Cells

T. Frei[1,†], C.-H. Chang[1,†], M. Filo[1], and M. Khammash[1,*]

[1]Department of Biosystems Science and Engineering, ETH Zürich, Switzerland
[†]These authors contributed equally.
[*]correspondence: mustafa.khammash@bsse.ethz.ch

December 6, 2020

Abstract

Mammalian cells collectively maintain a consistent internal milieu that supports their host's survival in varying and uncertain environments. This homeostasis is often achieved through negative feedback loops that act at various levels of biological organization, from the system and organ levels down to gene expression at the molecular scale. Recently, a molecular regulatory motif has been discovered that enables a regulated variable to adapt perfectly (at the steady state) to network and parameter changes and to persistent environmental perturbations. The regulatory motif that achieves this robust perfect adaptation property realizes integral feedback, a control strategy that employs mathematical integration in a negative feedback loop. Here, we present the first synthetic implementation of integral feedback in mammalian cells. We show that this implementation successfully maintains constant levels of a transcription factor, even when its degradation is significantly increased. Furthermore, we establish the structural robustness properties of our controlled system by demonstrating that perturbing the network topology does not affect the transcription factor levels. We believe that the ability to robustly and predictably regulate the expression levels of genes will both become an indispensable tool for basic research as well as lead to substantial advances in the development of industrial biotechnology and cell-based therapies.

Introduction

The ability to maintain a steady internal environment in the presence of a changing and uncertain external environment — called homeostasis — is a defining characteristic of living systems [1]. Homeostasis is maintained by various regulatory mechanisms, often in the form of negative feedback loops. The concept of homeostasis is particularly relevant in physiology and medicine, where loss of homeostasis is often attributed to the development of disease [2, 3, 4]. In this regard, deepening the understanding of the molecular mechanisms that govern homeostasis will guide the development of novel treatments to address human diseases.

In engineering, the ability of a control system to robustly maintain a controlled dynamical system of interest in a desired state in spite of perturbations is routinely achieved through the use of integral negative feedback. In integral feedback, the deviation of the regulated output of a system from its desired level is measured and mathematically integrated over time and then used to drive the system's input in a way to counteract the deviations and drive them to zero [5]. Like a biological system in homeostasis, a system with integral feedback is known to reject constant disturbances and furthermore, it is able to perfectly track a desired level commonly referred to as the setpoint. More recently, it has become increasingly evident that integral feedback drives biological adaptation as well [6, 7, 8, 9, 10].

bioRxiv preprint doi: https://doi.org/10.1101/2020.12.06.412304; this version posted December 6, 2020. The copyright holder for this preprint (which was not certified by peer review) is the author/funder. All rights reserved. No reuse allowed without permission.

Over the last decade, several experimental studies have constructed genetic systems and cell-based therapies that implement negative feedback to mitigate disease [11, 12, 13, 14]. These, however, rely on simple negative feedback rather than integral feedback and are therefore not guaranteed to achieve precise and robust regulation. In 2016, Briat et al. introduced a biomolecular circuit topology that implements integral feedback control for general biomolecular systems [15]. Figure 1(a) depicts an abstract representation of this control motif. Central to this strategy — termed antithetic integral feedback — is the so-called annihilation (or sequestration) reaction between the two species that implement the controller (reaction with rate η in Figure 1(a)). The annihilation refers to the requirement that both controller species abolish each other's function when they interact. Another stringent requirement to achieve integral feedback is that the two controller species on their own remain fairly stable over time. Given these conditions, any network interconnected in a stable way with this antithetic integral controller will achieve robust adaptation (Figure 1).

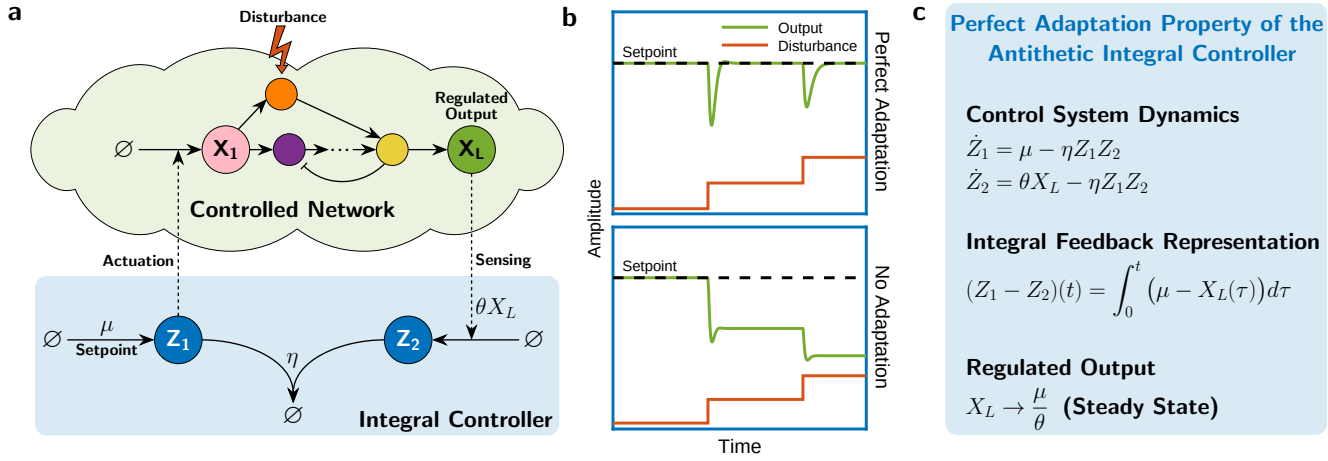

Figure 1: The Antithetic Integral Feedback Motif. (a) Network topology of an arbitrary molecular network with an embedded antithetic integral feedback motif. The nodes labelled with Z_1 and Z_2 together form the antithetic motif. Species Z_1 is produced at a rate μ and is functionally annihilated when it interacts with species Z_2 at a rate η. Furthermore, Z_1 interacts with the controlled network by promoting the production of species X_1. To close the feedback loop, species Z_2 is produced at a reaction rate that is proportional to θ and the regulated output species X_L. **(b) Comparison of open- and closed-loop dynamics.** In the absence of any disturbance to the controlled network, both the open- (bottom) and closed-loop (top) systems track the desired setpoint. However, when a disturbance occurs and persists, the open-loop circuit deviates from the desired setpoint while the closed-loop system returns after a transient deviation. **(c) Dynamics of the antithetic integral controller.** Subtracting the differential equations of Z_1 and Z_2 reveals the integral action of the controller that ensures that the steady state of the output converges to a value that is independent of the controlled network parameters.

This theoretical work has motivated the implementation of antithetic integral control in bacteria [16, 17] and in vitro [18]. A quasi-integral controller in *E. coli* [19] also relies on a similar topology. In realizing antithetic integral feedback, one of the main challenges is identifying a suitable implementation of the annihilation (or sequestration) reaction [17]. In the bacterial implementation of the antithetic integral feedback motif [17] stable proteins (a σ and anti-σ factor pair) were used to realize the sequestration reaction. However, this approach is not directly applicable to mammalian cells. Instead, in this work we exploit hybridization of complementary mRNAs to realize this critical reaction. (Figure 2(a)). For the antithetic integral controller to function properly, the sense and antisense RNAs have to be stable such that their degradation is predominantly due to their mutual interaction (via the hybridization reaction, see Figure 1(a)). Unlike bacterial RNAs where the majority of mRNAs have half-lives between 3 and 8 minutes [20], mammalian RNAs are much more stable with typical mRNA half lives of several hours [21]. Indeed in human cells, the majority of mRNAs have half-lives between 6 and 18 hours, with an overall mean value of 10 hours [22, 23]. The hybridization of the mammalian sense/antisense RNAs and their stability allow us to realize the antithetic integral controller in mammalian cells. Sense and antisense mRNA have previously been employed to control gene expression in yeast [24] and to build a genetic oscillator in mammalian cells [25]. Furthermore, antisense RNA has shown promise in the treatment of cancer and other genetic diseases as well as infections [26, 27, 28].

bioRxiv preprint doi: https://doi.org/10.1101/2020.12.06.412304; this version posted December 6, 2020. The copyright holder for this preprint (which was not certified by peer review) is the author/funder. All rights reserved. No reuse allowed without permission.

Here, we demonstrate perfect adaptation in a sense/antisense mRNA implementation of the antithetic integral feedback circuit in mammalian cells and show that the resulting closed-loop control system is highly robust to network changes and parameter disturbances. Furthermore, we derive a mathematical (mechanistic) model that describes the various interactions in the system. We show that the obtained model fits the experimentally obtained data well, and is also capable of predicting the robustness features of our implementation of the antithetic integral controller.

Results

A schematic depiction of the sense/antisense RNA implementation of the antithetic integral feedback circuit is shown in Figure 2(a). The basic circuit consists of two genes, which are encoded on separate plasmids. The gene in the *activator plasmid* is the synthetic transcription factor tTA (tetracycline transactivator) [29] fused to the fluorescent protein mCitrine. The expression of this gene is driven by the strong mammalian EF-1 α promoter. This transcription factor drives the expression of the other gene in the *antisense plasmid* via the tTA-responsive TRE promoter. This gene expresses an antisense RNA that is complementary to the *activator* mRNA. The hybridization of these two species realizes the annihilation reaction and closes the feedback loop. As a experimental control incapable of producing integral feedback, we built an open-loop analog of the closed-loop circuit, in which the TRE promoter was replaced by a non-cognate promoter. The closed-loop configuration is set up to regulate the expression levels of the *activator* tTA-mCitrine. To introduce specific perturbations to the *activator* we additionally fused an Asunaprevir (ASV) inducible degradation tag (SMASh) to tTA-mCitrine [30].

To show that our genetic implementation of the circuit performs integral feedback we apply constant disturbances with ASV at a concentration of 0.033 µM to HEK293T cells which were transiently transfected with either the open- or the closed-loop circuit. Additionally, we vary the setpoint by transfecting the two plasmids at ratios ranging from 1/16 to 1/2 (Activator Plasmid/Antisense Plasmid). The fluorescence of the cells was measured 48 hours after transfection using flow cytometry. As the setpoint ratio increases, so does the fluorescence of tTA-mCitrine, indicating that our circuit permits setpoint control (Figure 2(b)). Note that this fluorescence is a monotonically-increasing function of the plasmid ratios (see also the function θ in Figure 4(b)). We consider a circuit to be adapting if its normalized fluorescence intensity stays within 10% of the undisturbed control. Under this criterion, adaptation is achieved for all the setpoints tested in the closed-loop configuration, whereas none of the open-loop configurations manage to meet our criteria for adaptation (Figure 2(c)). We note that adaptation for this circuit is also achieved at higher plasmid ratios (Figure 4(c)).

Next, we sought to demonstrate that our implementation of the antithetic integral controller will provide disturbance rejection at different setpoints regardless of the network topology it regulates. Therefore, we added a negative feedback loop from tTA-mCitrine to its own production. This negative feedback was realized by the RNA-binding protein L7Ae [31], which is expressed under the control of a tTA-responsive TRE promoter and binds the kink-turn hairpin on the sense mRNA to inhibit translation (Figure 3(a)). The closed- and open-loop circuits were transiently transfected either with or without this negative feedback plasmid to introduce a perturbation to the regulated network. As before, the setpoints 1/2 and 1 were tested by transfecting an appropriate ratio of the *activator* to *antisense* plasmids. These different conditions were further perturbed on the molecular level by adding 0.033 µM ASV to induce degradation of tTA-mCitrine. As shown in Figure 3(b) the closed-loop circuit rejects both perturbations in most cases, whereas again the open-loop circuit fails to adapt. However, the closed-loop circuit with a setpoint of 1/2 with both perturbations also fails to meet our adaptation requirement. Nevertheless, it still outperforms the open-loop circuit under the same conditions.

To demonstrate that the circuit in Figure 2(a) is consistent with our understanding of the regulation topology, we derive a detailed mechanistic model starting from basic principles of mass-action kinetics. A mechanistic model can be presented as a biochemical reaction network that describes the interactions between the various species in the circuit. However, to simplify the mathematical model, a model reduction technique is carried out based on a quasi-steady-state approximation that exploits a time-

bioRxiv preprint doi: https://doi.org/10.1101/2020.12.06.412304; this version posted December 6, 2020. The copyright holder for this preprint (which was not certified by peer review) is the author/funder. All rights reserved. No reuse allowed without permission.

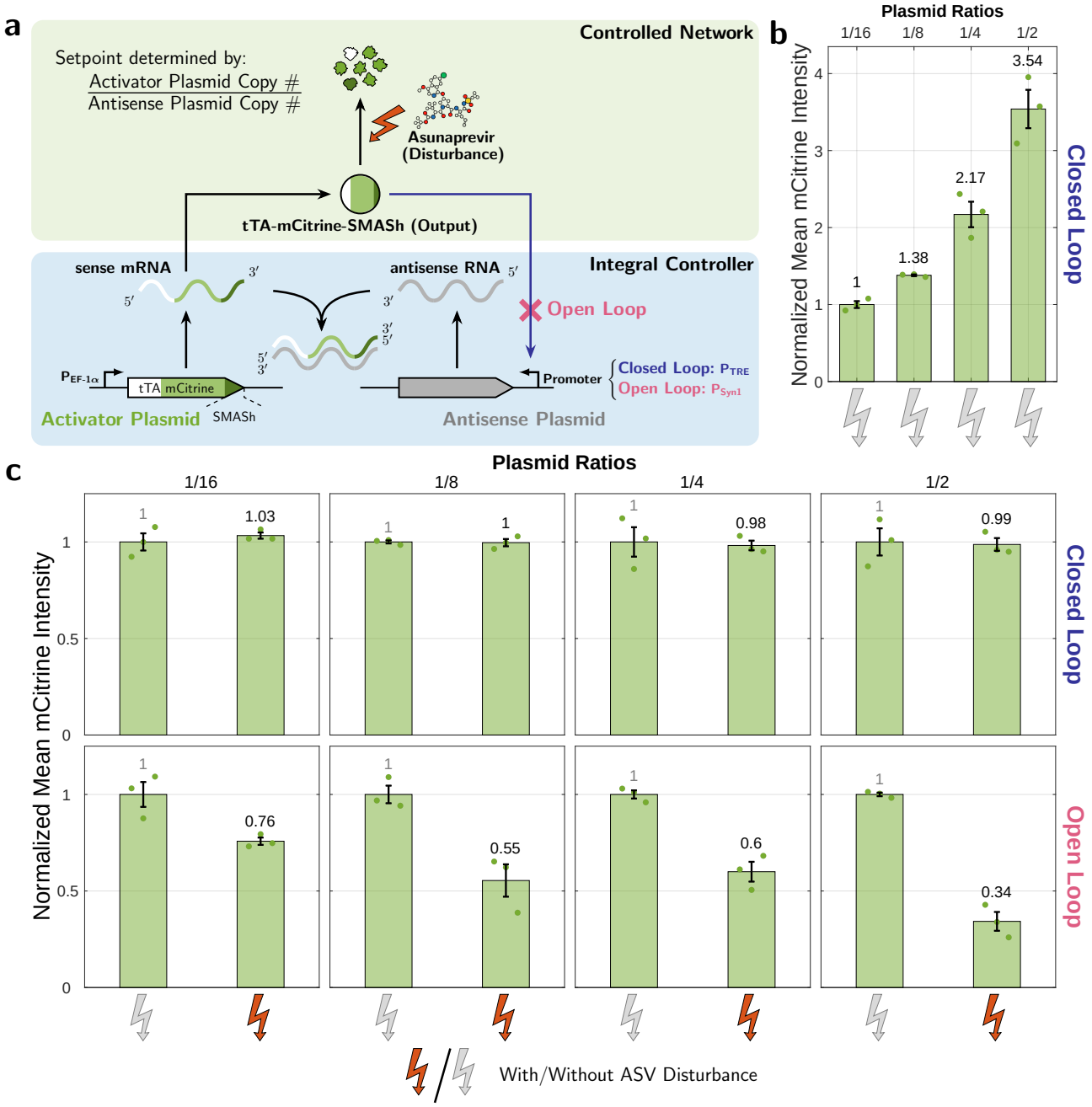

Figure 2: Perfect Adaptation of a Synthetic Antithetic Integral Feedback Circuit in Mammalian Cells. (a) Genetic implementation of open- and closed-loop circuits. Both circuits consist of two genes, realized on separate plasmids. The gene in the *activator plasmid* encodes the synthetic transcription factor tTA (tetracycline transactivator) tagged with the fluorescent protein mCitrine and a chemically-inducible degradation tag (SMASh). Its expression is driven by a strong constitutive promoter ($P_{EF\text{-}1\ \alpha}$). The gene in the *antisense plasmid* expresses the antisense RNA under the control of a tTA responsive promoter (P_{TRE}). In the open-loop configuration, the TRE promoter was exchanged for a non-cognate promoter. In this setting the controlled species is the tTA protein, which can be perturbed externally by addition of Asunaprevir (ASV), the chemical inducer of the SMASh degradation tag. **(b) Steady-state levels of the output (mCitrine) under increasing plasmid ratios.** The genetic implementation of the closed-loop circuit as shown in panel (a) was transiently transfected at different molar ratios (setpoint := *activator* / *antisense*) by varying the concentration of the activator plasmid while keeping the concentration of the antisense plasmid constant. The data was collected 48 hours after transfection and is shown as mean per condition normalized to the lowest setpoint (1/16) ± s.e. for n = 3 replicates. This shows that increasing the plasmid ratio increases the steady-state output level. **(c) Steady-state response of the open-loop and closed-loop implementations to induced degradation by ASV.** The genetic implementation of the open- and closed-loop circuit as shown in panel (a) was transiently transfected at different molar ratios and perturbed with 0.033 µM of ASV. The data was collected 48 hours after transfection and is shown as mean per condition normalized to the unperturbed conditions for each setpoint separately. This demonstrates the disturbance rejection capability of the closed-loop circuit and shows that the open-loop circuit fails to achieve adaptation.

bioRxiv preprint doi: https://doi.org/10.1101/2020.12.06.412304; this version posted December 6, 2020. The copyright holder for this preprint (which was not certified by peer review) is the author/funder. All rights reserved. No reuse allowed without permission.

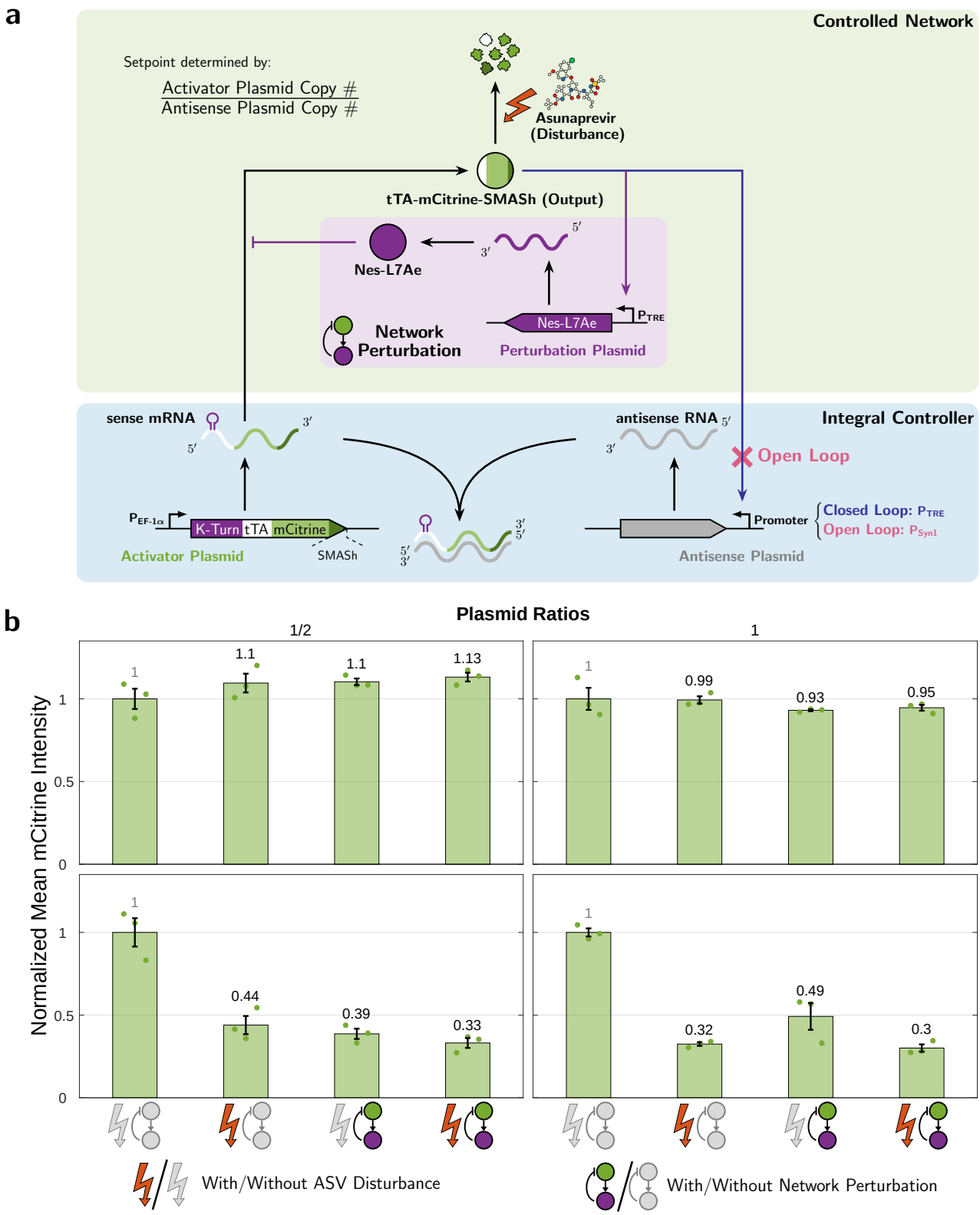

Figure 3: Perturbation to the Controlled Network. (a) Extension of the network topology with a negative feedback loop. A negative feedback loop from tTA-mCitrine to its own production was added by expressing the RNA-binding protein L7Ae under the control of a tTA-responsive TRE promoter. This protein binds to the kink-turn hairpin on the sense mRNA to inhibit the translation of tTA. **(b) The closed-loop circuit is not affected by the topology of the regulated network.** The closed- and open-loop circuits were perturbed by co-transfecting the *network perturbation* plasmid and by adding 0.033 µM of ASV. This was done at two setpoints 1/2 and 1 (setpoint := *activator* / *antisense*). The HEK293T cells were measured using flow cytometry 48 hours after transfection and the data is shown as mean per condition normalized to the unperturbed network and no ASV condition ± s.e. for n = 3 replicates.

bioRxiv preprint doi: https://doi.org/10.1101/2020.12.06.412304; this version posted December 6, 2020. The copyright holder for this preprint (which was not certified by peer review) is the author/funder. All rights reserved. No reuse allowed without permission.

scale separation principle imposed by the various fast binding/unbinding reactions in the network. The resulting reduced model, depicted in Figure 4(a), can be divided into a controller sub-network that is connected in feedback with another sub-network to be controlled. This is illustrated schematically in Figure 4(a) and mathematically as a set of ordinary differential equations (ODEs) in Figure 4(b), where uppercase letters denote concentrations of the corresponding species (in bold fonts). The reduced model captures the expression dynamics of the two genes, denoted by $\mathbf{G_1}$ and $\mathbf{G_2}$, that are encoded in the activator and antisense plasmids, respectively. Note that the active degradation of $\mathbf{X_1}$ by $\mathbf{D}$ is mathematically represented by the function λ given in Figure 4(b) which is linear in D but nonlinear in X_1. This nonlinearity can be of lower order (set $k_3' = 0$ and $\kappa_3' \to \infty$ to obtain a first order hill function $\lambda(X_1; D) = k_3 D \frac{X_1/\kappa_3}{1+X_1/\kappa_3}$) or higher order ($k_3' > 0$ and $\kappa_3' < \infty$) if the fusion protein tTA-mCitrine-SMASh can still dimerize before it releases the SMASh tag.

Next, we calibrated the obtained mathematical model to the experimental measurements that are collected at steady state. The measured fluorescence, denoted by M, represents all the molecules involving mCitrine: $\mathbf{X_1}$ $\mathbf{X_2}$, and $\mathbf{A}$. It can be shown that M can be expressed solely in terms of the concentration of the regulated output $\mathbf{A}$ as shown in the bottom of Figure 4(c), where c_G is an instrument-related proportionality constant that maps concentrations in nM to fluorescence in a.u., and κ is the dimerization dissociation constant of $\mathbf{A}$. Of course, steady-state measurements alone cannot uniquely estimate all parameters in the model. However, by carrying out a steady-state analysis of the differential equations in Figure 4(b), we can identify a set of parameter groups (or lumped parameters) that can be uniquely estimated based on the collected data. In the ideal closed-loop scenario where the dilution rate is zero, the steady-state analysis is fairly straight forward and is shown in the bottom of Figure 4(b). This analysis shows that the steady-state concentration of the regulated output, denoted by $\bar{A}$, is a monotonically increasing function of the plasmid ratio G_1/G_2, and is independent of the various controlled network parameters, particularly the disturbance D. As a result, robust perfect adaptation is exactly achieved since ASV disturbance has absolutely no effect on the steady-state concentration of the regulated output $\mathbf{A}$. In practice, the dilution/degradation rate δ is never exactly zero, which makes the integrator 'leaky'. In this case, the steady-state analysis becomes more involved, and one cannot obtain an explicit formula for $\bar{A}$ as in the ideal situation. However, implicit (polynomial) formulae can be obtained and are used here to fit the mathematical model to the data. It should be pointed out that when δ is sufficiently small relative to other controller rate parameters (as can be achieved with slowly growing cells and fairly stable sense/antisense RNA) the integrator leakiness will be small, and perfect adaption can still be achieved for all practical purposes [17, 32]. This can be seen experimentally in Figure 2. The model fits, shown in Figure 4(c), are carried out sequentially for the open-loop circuit first (with and without disturbance) then the closed-loop circuit (without disturbance). This sequential procedure avoids over-fitting the model to the data. Finally, the closed-loop c ircuit with disturbance is left for model prediction to assess the accuracy of the estimated model. As shown in Figure 4(c), the model fits the data very well, and is also capable of predicting the experimentally observed disturbance rejection feature of the antithetic integral controller.

Next, consider the circuit in Figure 3(a), where an additional gene is added as a network perturbation that introduces a feedback in the controlled network. By introducing the additional biochemical reactions to the previous circuit of Figure 2(a) and carrying out the same model reduction technique, it is shown that a sub-network of biochemical reactions (shown in purple in Figure 5(a)) is appended to the previously obtained reduced model of Figure 4(a). This appended sub-network captures the expression dynamics of the additional perturbation gene denoted by $\mathbf{G_2'}$. The updated ODEs are depicted in Figure 5(b). Next, we calibrate the updated mathematical model to the experimental measurements that are collected at steady state. Once again, we identify the additional set of parameter groups (or lumped parameters) that arise due to the network perturbation. In the ideal closed-loop scenario where δ is zero, the steady-state concentration of the regulated output $\bar{A}$ is, once again, completely unaffected by the network perturbation as illustrated in the bottom of Figure 5(b). This demonstrates that the antithetic integral controller is not only capable of rejecting disturbances, but is also robust to network perturbations as well. As previously, the model we use here allows $\delta \neq 0$, and the model fitting, shown in Figure 5(c), is carried out sequentially to avoid over-fitting. First, the relevant parameter groups that were obtained

bioRxiv preprint doi: https://doi.org/10.1101/2020.12.06.412304; this version posted December 6, 2020. The copyright holder for this preprint (which was not certified by peer review) is the author/funder. All rights reserved. No reuse allowed without permission.

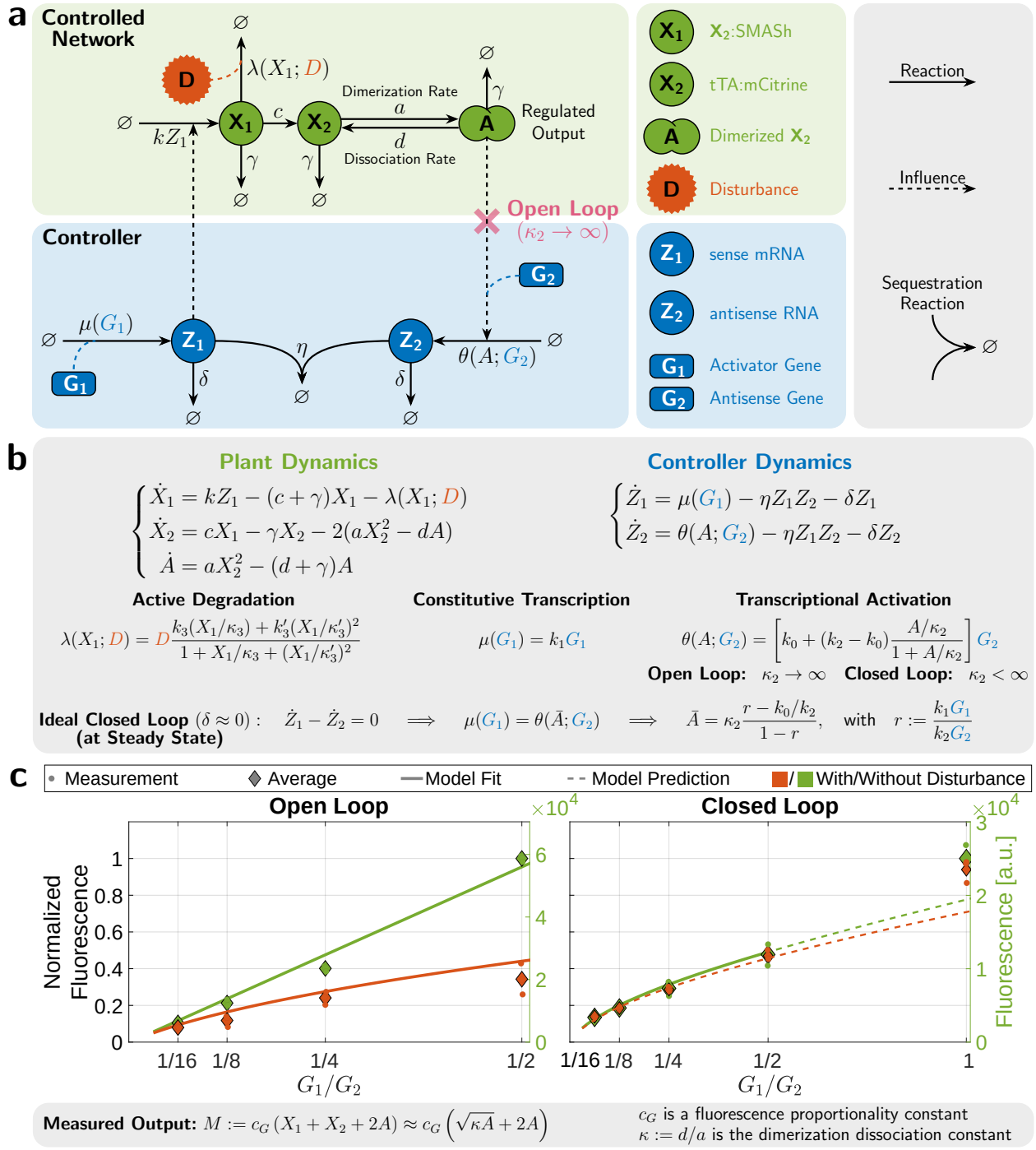

Figure 4: Mathematical Modeling of the Circuit in Figure 2. (a)/(b) Schematic/Mathematical Description of the Reduced Model. The sense mRNA, $\mathbf{Z_1}$, is constitutively produced at a rate $\mu(G_1)$ that depends on the gene (plasmid) concentration, G_1. Then, $\mathbf{Z_1}$ is translated into a fluorescent protein $\mathbf{X_1}$, at a rate k, which is either actively degraded by the ASV disturbance $\mathbf{D}$ at a rate $\lambda(X_1; D)$ or converted to $\mathbf{X_2}$ at a rate c by releasing the SMASh tag. The protein $\mathbf{X_2}$ dimerizes to form $\mathbf{A}$ which acts as a transcription factor that activates the transcription of the antisense RNA, $\mathbf{Z_2}$. The transcription rate, denoted by θ, is a function of A and the gene concentration G_2. The antithetic integral control is realized by the sequestration of $\mathbf{Z_1}$ and $\mathbf{Z_2}$ at a rate η. Note that the open-loop circuit is obtained by setting $\kappa_2 \to \infty$, where κ_2 is the dissociation constant of $\mathbf{A}$ from $\mathbf{G_2}$. This removes the feedback from the regulated output A since $\theta(A; G_2)$ becomes $k_0 G_2$. In the ideal operation of the antithetic integral controller, where the dilution rate δ is zero, the steady-state concentration of $\mathbf{A}$, denoted by $\bar{A}$, is independent of the controlled network parameters. This independence ensures robust perfect adaptation of the regulated output to external disturbances, such as $\mathbf{D}$. **(c) Model Fitting to Experimental Data.** The left plot shows the model fit for the open-loop circuit with/without disturbance. The right plot shows the model fit for the closed-loop circuit without disturbance. The dashed line represents a model prediction for the closed-loop circuit with disturbance. The model fits and prediction show a very good agreement with the experiments over a wide range of plasmid ratios (setpoints) G_1/G_2 (with/without disturbance).

bioRxiv preprint doi: https://doi.org/10.1101/2020.12.06.412304; this version posted December 6, 2020. The copyright holder for this preprint (which was not certified by peer review) is the author/funder. All rights reserved. No reuse allowed without permission.

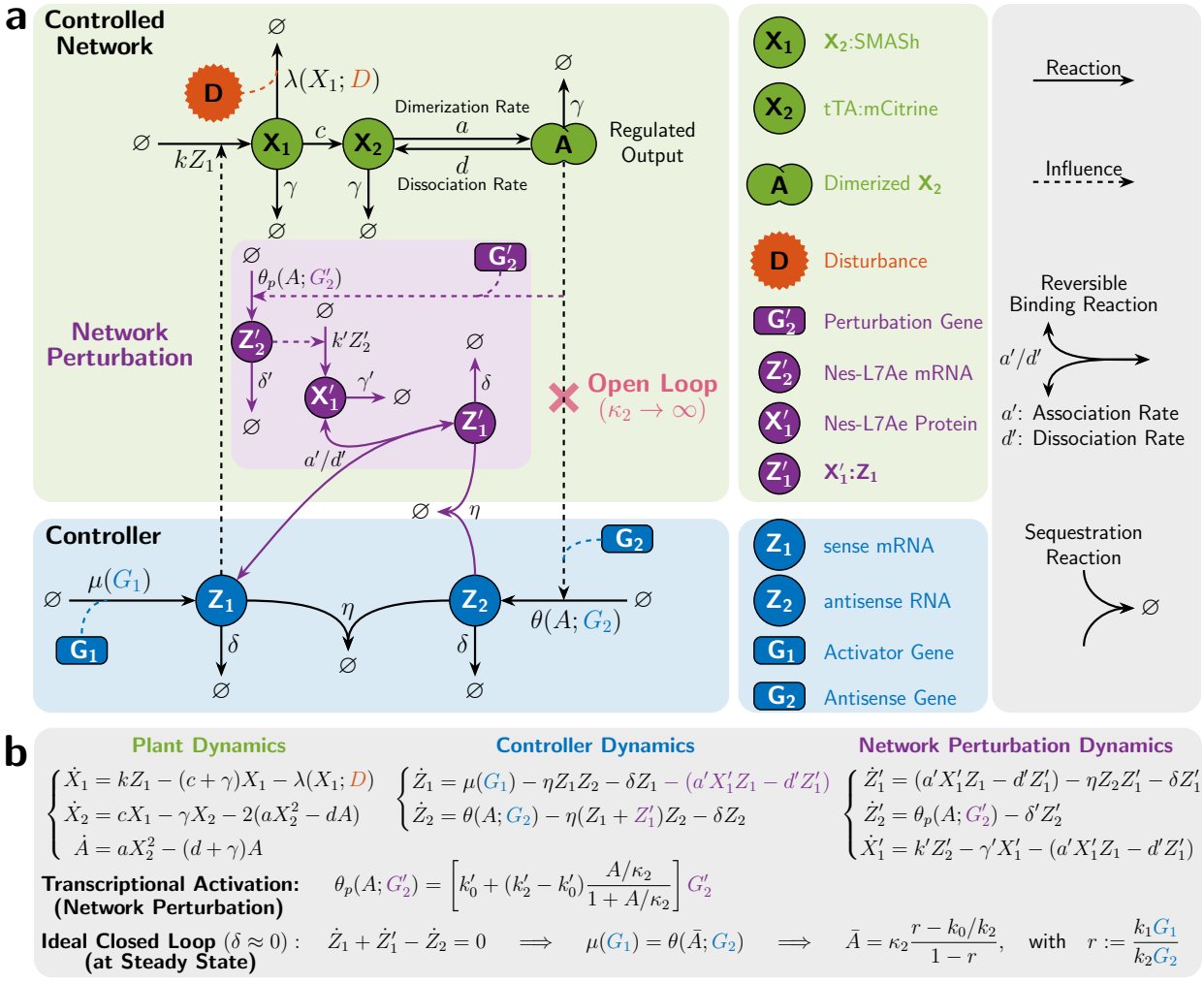

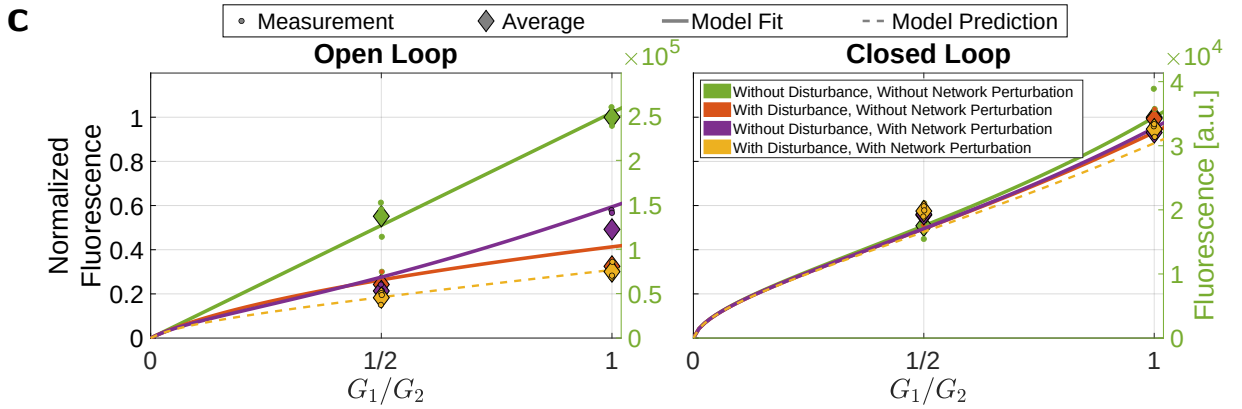

Figure 5: Mathematical Modeling of the Circuit in Figure 3. (a)/(b) Schematic/Mathematical Description of the Reduced Model. The network perturbation introduced by the additional Nes-L7Ae gene, denoted by $\mathbf{G_2'}$, appends the sub-network in purple to the previously obtained reduced model in Figure 2(a). Here, the dimer $\mathbf{A}$ acts as a transcription factor for both genes $\mathbf{G_2}$ and $\mathbf{G_2'}$. When $\mathbf{G_2'}$ is activated, it is transcribed into $\mathbf{Z_2'}$ at a rate $\theta_p(X_2; G_2')$ which in turn is translated into $\mathbf{X_1'}$ at a rate $k'Z_2'$. Then $\mathbf{X_1'}$ is capable of inhibiting the translation of $\mathbf{Z_1}$ by binding to it. Note that the complex $\mathbf{Z_1'}$ formed from the binding reaction can still sequester the antisense RNA $\mathbf{Z_2}$. In the ideal operation of the antithetic integral controller, where the dilution rate δ is negligible with respect to the other rates of the controller, the regulated output $\mathbf{A}$ has a steady-state concentration, denoted by $\bar{A}$, that is unaffected by the network perturbation. This ensures robust perfect adaptation of the output not only to external disturbances in the controlled network as illustrated in Figure 2, but also to network perturbations as well. **(c) Model Fitting to Experimental Data.** The plots show the model fits obtained for both open- and closed-loop circuits with and without disturbance and/or network perturbation for two plasmid ratios (setpoints) $G_1/G_2 = 1/2$ and 1. The dashed line represents a model prediction in the presence of both disturbance D and network perturbation via $\mathbf{G_2'}$. The model fits and predictions show a very good agreement with the experimentally collected measurements for both open- and closed-loop circuits.

bioRxiv preprint doi: https://doi.org/10.1101/2020.12.06.412304; this version posted December 6, 2020. The copyright holder for this preprint (which was not certified by peer review) is the author/funder. All rights reserved. No reuse allowed without permission.

from the previous model fit (without network perturbation) are re-calibrated to the new experimental conditions. Then, the new parameters that are related to the sub-network introduced by the perturbation gene $\mathbf{G_2'}$ are estimated to yield the solid purple curves. Finally, the open- and closed-loop circuits with both disturbance and network perturbation are left for model prediction to assess the accuracy of the estimated model. As shown in Figure 5(c), fits the data quite well, and is also capable of predicting the experimentally observed features of the antithetic integral controller (disturbance rejection and robustness to network perturbations).

Discussion

The presented study demonstrates the first implementation of antithetic integral feedback in mammalian cells. With our proof-of-principle circuit we lay the foundation for robust and predictable control systems engineering in mammalian biology. We believe integral feedback systems will have a transformative effect on the field of synthetic biology just like they have had on other engineering disciplines.

Based on the antithetic motif (Figure 1(a)), we designed and built a proof-of-concept circuit capable of perfect adaptation. This was achieved by exploiting the hybridization of mRNA molecules to complementary antisense RNAs. The resulting inhibition of translation realizes the central sequestration mechanism. Specifically, we express an antisense RNA through a promoter that is activated by the transcription factor tTA. This antisense RNA is complementary to and binds the mRNA of tTA to close the negative feedback loop (Figure 2(a)). We further highlight the properties of integral feedback control by showing that our circuit permits different setpoints. By applying a disturbance to the regulated species we have shown that the closed-loop circuit achieves adaptation and provides superior robustness compared to an analogous open-loop circuit (2(c)). Further, we showed that adaptation is also achieved when the setpoint of the circuit is changed.

Moreover, we also showed that our realization of the antithetic integral feedback motif is agnostic to the network structure of the regulated species. This was achieved by introducing a perturbation to the controlled network itself(Figure 3(b)). Furthermore, we also demonstrated that the closed-loop circuit still rejects disturbances even in the presence of this extra perturbation to the network. In the open-loop circuit, the disturbance, perturbation and perturbation with disturbance lead to a successively stronger decrease in tTA-mCitrine expression.

Finally, we derived mechanistic mathematical models for the circuits, starting from basic mass-action kinetics, and showed that the obtained models are capable of fitting the experimental measurements fairly well. We also showed that the models are capable of predicting the features of our implementation of the antithetic integral controller: disturbance rejection and robustness to network perturbations.

An earlier implementation of the antithetic integral feedback motif in bacteria [17] used a σ and anti-σ factor pair to realize the sequestration reaction. Due to the requirement of factors native to the bacterial cell for σ factors to activate transcription, this approach is not directly applicable to mammalian cells. Conversely, the sense and antisense RNA approach utilized in this study is likely to be more difficult to realize in bacterial cells due to rapid mRNA turnover.

In light of recent studies on the effects of shared cellular resources in mammalian cells [33, 34], it is important to point out that the dependence of the production of the two controller species on the same resource pool (e.g. transcriptional resources for sense/antisense RNAs) is crucial for maintaining the setpoint despite variations in resource availability. This derives from the fact that the setpoint is a function of the ratio of the production rates of the two controller species (ratio r in Figures 4(b) and 5(b)). If both rates depend on the same resource pool, then the dependence on these resources cancel each other out. When the production rates depend on different resource pools they do not cancel out and the setpoint becomes sensitive to resource allocation.

Aside from realizing integral feedback control, the sense and antisense RNA implementation is very simple to adapt and is versatile. Indeed both sense and antisense are fully programmable, with the only

bioRxiv preprint doi: https://doi.org/10.1101/2020.12.06.412304; this version posted December 6, 2020. The copyright holder for this preprint (which was not certified by peer review) is the author/funder. All rights reserved. No reuse allowed without permission.

requirement that they share sufficient sequence homology to hybridize and inhibit translation. Due to this, mRNAs of endogenous transcription factors may easily be converted into the antithetic motif simply by expressing their antisense RNA from a promoter activated by the transcription factor. However, one should note, that in this case the setpoint to the transcription factor will be lower than without the antisense RNA due to the negative feedback and additionally, if the mRNA of the endogenous transcription factor is not very stable, the integrator is expected to not perform optimally.

We believe that the ability to precisely and robustly regulate gene expression in mammalian cells will find many applications in industrial biotechnology and biomedicine. In the area of biomedicine, these robust perfectly adapting controllers can be used to restore homeostasis in the treatment of metabolic diseases, as well as for applications in immunotherapy and precise drug delivery.

Methods

Plasmid construction

Plasmids for transfection were constructed using a mammalian adaption of the modular cloning (MoClo) yeast toolkit standard [35]. Custom parts for the toolkit were generated by PCR amplification (Phusion Flash High-Fidelity PCR Master Mix; Thermo Scientific) and assembled into toolkit vectors via golden gate assembly [36]. All enzymes used for applying the MoClo procedure were obtained from New England Biolabs (NEB).

Cell culture

HEK293T cells (ATCC, strain number CRL-3216) were cultured in Dulbecco's modified Eagle's medium (DMEM; Gibco) supplemented with 10 % FBS (Sigma-Aldrich), 1x GlutaMAX (Gibco) and 1 mM Sodium Pyruvate (Gibco). The cells were maintained at 37 °C and 5 % CO_2. Every 2 to 3 days the cells were passaged into a fresh T25 flask. When required, surplus cells were plated for transfection.

Transfection

Cells used in transfection experiments were plated in a 96 wells plate at 10,000–15,000 cells per well approximately 24 h before treatment with the transfection solution. The transfection solution was prepared using Polyethylenimine (PEI) "MAX" (MW 40000; Polysciences, Inc.) at a 1:3 (µg DNA to µg PEI) ratio with a total of 100 ng plasmid DNA per well. The solution was prepared in Opti-MEM I (Gibco) and incubated for approximately 25 min prior to addition to the cells.

Flow cytometry

Approximately 48 h after transfection the cells were collected in 60 µL Accutase solution (Sigma-Aldrich). The fluorescence was measured on a Beckman Coulter CytoFLEX S flow cytometer using the 488 nm laser with a 525/40+OD1 bandpass filter. For each sample the whole cell suspension was collected. In each measurement additional unstained and single color (mCitrine only) controls were collected for gating and compensation.

Data analysis

The acquired data was analyzed using a custom analysis pipeline implemented in the R programming language. The measured events are automatically gated and compensated for further plotting and analysis.

bioRxiv preprint doi: https://doi.org/10.1101/2020.12.06.412304; this version posted December 6, 2020. The copyright holder for this preprint (which was not certified by peer review) is the author/funder. All rights reserved. No reuse allowed without permission.

Acknowledgments

We thank Dr. Gabriele Lillacci for his support during the early stage of the project. We also thank Drs. Stephanie Aoki and Ankit Gupta for reading the manuscript and providing many useful comments.

Competing interests

ETH Zürich has filed a patent application on behalf of the inventors T.F., C.H.C., M.F. and M.K. on the genetic circuit designs described (application no. EP20206417.6).

References

[1] Lisa A Urry, Michael Lee Cain, Steven Alexander Wasserman, Peter V Minorsky, and Jane B Reece. *Campbell biology*. Pearson Education, Incorporated, 2017.

[2] Maya E. Kotas and Ruslan Medzhitov. Homeostasis, inflammation, and disease susceptibility. *Cell*, 160(5):816–827, 2015.

[3] Rashmi Mullur, Yan-Yun Liu, and Gregory A Brent. Thyroid hormone regulation of metabolism. *Physiological reviews*, 94(2):355–382, 2014.

[4] Fa-Xing Yu, Bin Zhao, and Kun-Liang Guan. Hippo pathway in organ size control, tissue homeostasis, and cancer. *Cell*, 163(4):811–828, 2015.

[5] Karl Johan Åström and Richard M Murray. *Feedback systems: an introduction for scientists and engineers*. Princeton university press, 2010.

[6] T.-M. Yi, Y. Huang, M. I. Simon, and J. Doyle. Robust perfect adaptation in bacterial chemotaxis through integral feedback control. *Proceedings of the National Academy of Sciences*, 97(9):4649–4653, 2000.

[7] H. El-Samad, J.P. Goff, and M. Khammash. Calcium homeostasis and parturient hypocalcemia: an integral feedback perspective. *Journal of Theoretical Biology*, 214(1):17–29, 2002.

[8] Paul Miller and Xiao-Jing Wang. Inhibitory control by an integral feedback signal in prefrontal cortex: a model of discrimination between sequential stimuli. *Proceedings of the National Academy of Sciences*, 103(1):201–206, 2006.

[9] Dale Muzzey, Carlos A Gómez-Uribe, Jerome T Mettetal, and Alexander van Oudenaarden. A systems-level analysis of perfect adaptation in yeast osmoregulation. *Cell*, 138(1):160–171, 2009.

[10] Danny Ben-Zvi and Naama Barkai. Scaling of morphogen gradients by an expansion-repression integral feedback control. *Proceedings of the National Academy of Sciences*, 107(15):6924–6929, 2010.

[11] Christian Kemmer, Marc Gitzinger, Marie Daoud-El Baba, Valentin Djonov, Jörg Stelling, and Martin Fussenegger. Self-sufficient control of urate homeostasis in mice by a synthetic circuit. *Nature biotechnology*, 28(4):355, 2010.

[12] Ping Wei, Wilson W Wong, Jason S Park, Ethan E Corcoran, Sergio G Peisajovich, James J Onuffer, Arthur Weiss, and Wendell A Lim. Bacterial virulence proteins as tools to rewire kinase pathways in yeast and immune cells. *Nature*, 488(7411):384–388, 2012.

[13] Katrin Rössger, Ghislaine Charpin-El-Hamri, and Martin Fussenegger. A closed-loop synthetic gene circuit for the treatment of diet-induced obesity in mice. *Nature communications*, 4(1):1–9, 2013.

bioRxiv preprint doi: https://doi.org/10.1101/2020.12.06.412304; this version posted December 6, 2020. The copyright holder for this preprint (which was not certified by peer review) is the author/funder. All rights reserved. No reuse allowed without permission.

[14] Mingqi Xie, Haifeng Ye, Hui Wang, Ghislaine Charpin-El Hamri, Claude Lormeau, Pratik Saxena, Jörg Stelling, and Martin Fussenegger. β-cell–mimetic designer cells provide closed-loop glycemic control. *Science*, 354(6317):1296–1301, 2016.

[15] Corentin Briat, Ankit Gupta, and Mustafa Khammash. Antithetic integral feedback ensures robust perfect adaptation in noisy biomolecular networks. *Cell Systems*, 2(1):15–26, 2016.

[16] Gabriele Lillacci, Stephanie Aoki, David Schweingruber, and Mustafa Khammash. A synthetic integral feedback controller for robust tunable regulation in bacteria. *Biorxiv*, page 170951, 2017.

[17] Stephanie K. Aoki, Gabriele Lillacci, Ankit Gupta, Armin Baumschlager, David Schweingruber, and Mustafa Khammash. A universal biomolecular integral feedback controller for robust perfect adaptation. *Nature*, 570(7762):533–537, 2019.

[18] Deepak K Agrawal, Ryan Marshall, Vincent Noireaux, and Eduardo D Sontag. In vitro implementation of robust gene regulation in a synthetic biomolecular integral controller. *Nature communications*, 10(1):1–12, 2019.

[19] Hsin-Ho Huang, Yili Qian, and Domitilla Del Vecchio. A quasi-integral controller for adaptation of genetic modules to variable ribosome demand. *Nature Communications*, 9(1):5415, 2018.

[20] Ron Milo and Rob Phillips. *Cell biology by the numbers*. Garland Science, 2015.

[21] José E Pérez-Ortín, Paula Alepuz, Sebastián Chávez, and Mordechai Choder. Eukaryotic mrna decay: methodologies, pathways, and links to other stages of gene expression. *Journal of molecular biology*, 425(20):3750–3775, 2013.

[22] Edward Yang, Erik van Nimwegen, Mihaela Zavolan, Nikolaus Rajewsky, Mark Schroeder, Marcelo Magnasco, and James E Darnell. Decay rates of human mrnas: correlation with functional characteristics and sequence attributes. *Genome research*, 13(8):1863–1872, 2003.

[23] Björn Schwanhäusser, Dorothea Busse, Na Li, Gunnar Dittmar, Johannes Schuchhardt, Jana Wolf, Wei Chen, and Matthias Selbach. Global quantification of mammalian gene expression control. *Nature*, 473(7347):337–342, 2011.

[24] Travis S Bayer and Christina D Smolke. Programmable ligand-controlled riboregulators of eukaryotic gene expression. *Nature biotechnology*, 23(3):337–343, 2005.

[25] Marcel Tigges, Tatiana T. Marquez-Lago, Jörg Stelling, and Martin Fussenegger. A tunable synthetic mammalian oscillator. *Nature*, 457(7227):309–312, 2009.

[26] Rebecca P Haberman, Hugh E Criswell, Stephen Snowdy, Zhen Ming, George R Breese, R Jude Samulski, and Thomas J McCown. Therapeutic liabilities of in vivo viral vector tropism: adeno-associated virus vectors, nmdar1 antisense, and focal seizure sensitivity. *Molecular Therapy*, 6(4):495–500, 2002.

[27] Bryan C Fuchs, J Christian Perez, Julie E Suetterlin, Sofia B Chaudhry, and Barrie P Bode. Inducible antisense rna targeting amino acid transporter atb0/asct2 elicits apoptosis in human hepatoma cells. *American Journal of Physiology-Gastrointestinal and Liver Physiology*, 286(3):G467–G478, 2004.

[28] Pablo Tebas, David Stein, Gwendolyn Binder-Scholl, Rithun Mukherjee, Troy Brady, Tessio Rebello, Laurent Humeau, Michael Kalos, Emmanouil Papasavvas, Luis J Montaner, et al. Antiviral effects of autologous cd4 t cells genetically modified with a conditionally replicating lentiviral vector expressing long antisense to hiv. *Blood, The Journal of the American Society of Hematology*, 121(9):1524–1533, 2013.

[29] Manfred Gossen and Hermann Bujard. Tight control of gene expression in mammalian cells by tetracycline-responsive promoters. *Proceedings of the National Academy of Sciences*, 89(12):5547–5551, 1992.

bioRxiv preprint doi: https://doi.org/10.1101/2020.12.06.412304; this version posted December 6, 2020. The copyright holder for this preprint (which was not certified by peer review) is the author/funder. All rights reserved. No reuse allowed without permission.

[30] Hokyung K Chung, Conor L Jacobs, Yunwen Huo, Jin Yang, Stefanie A Krumm, Richard K Plemper, Roger Y Tsien, and Michael Z Lin. Tunable and reversible drug control of protein production via a self-excising degron. *Nature chemical biology*, 11(9):713–720, 2015.

[31] Hirohide Saito, Tetsuhiro Kobayashi, Tomoaki Hara, Yoshihiko Fujita, Karin Hayashi, Rie Furushima, and Tan Inoue. Synthetic translational regulation by an l7ae–kink-turn rnp switch. *Nature chemical biology*, 6(1):71–78, 2010.

[32] Yili Qian and Domitilla Del Vecchio. Realizing 'integral control'in living cells: how to overcome leaky integration due to dilution? *Journal of The Royal Society Interface*, 15(139):20170902, 2018.

[33] Timothy Frei, Federica Cella, Fabiana Tedeschi, Joaquín Gutiérrez, Guy-Bart Stan, Mustafa Khammash, and Velia Siciliano. Characterization and mitigation of gene expression burden in mammalian cells. *Nature Communications*, 11(1):4641, Sep 2020.

[34] Ross D. Jones, Yili Qian, Velia Siciliano, Breanna DiAndreth, Jin Huh, Ron Weiss, and Domitilla Del Vecchio. An endoribonuclease-based feedforward controller for decoupling resource-limited genetic modules in mammalian cells. *Nature Communications*, 11(1):5690, Nov 2020.

[35] Michael E Lee, William C DeLoache, Bernardo Cervantes, and John E Dueber. A highly characterized yeast toolkit for modular, multipart assembly. *ACS synthetic biology*, 4(9):975–986, 2015.

[36] Carola Engler, Romy Kandzia, and Sylvestre Marillonnet. A one pot, one step, precision cloning method with high throughput capability. *PloS one*, 3(11), 2008.